

# EFFECT OF B<sub>4</sub>C ADDITION ON THE MICROSTRUCTURE, HARDNESS AND DRY-SLIDING-WEAR PERFORMANCE OF AZ91 COMPOSITES PRODUCED WITH HOT PRESSING

## VPLIV DODATKA B<sub>4</sub>C NA MIKROSTRUKTURO, TRDOTO IN SUHO DRSNO OBRABO VROČE STISKANIH KOMPOZITOV AZ91

Taba Özdemir Öge<sup>1\*</sup>, Mecit Öge<sup>2</sup>, Volkan Murat Yılmaz<sup>3</sup>, Firdevs Banu Özdemir<sup>4</sup>

<sup>1</sup>Bartın University, Vocational School of Health Services, Ağdacı Campus, 74100, Bartın, Turkey

<sup>2</sup>Bartın University, Faculty of Engineering, Department of Mechanical Engineering, Kutlubey-Yazıcılar Campus, 74100, Bartın, Turkey

<sup>3</sup>Bartın University, Central Research Laboratory, Kutlubey-Yazıcılar Campus, 74100, Bartın, Turkey

<sup>4</sup>Beykent University, Department of Health Programmes, Buyukcekmece Premises, 34550, Istanbul, Turkey

*Prejem rokopisa – received: 2018-06-27; sprejem za objavo – accepted for publication: 2019-01-08*

doi:10.17222/mit.2018.127

AZ91-B<sub>4</sub>C composites were fabricated with varying reinforcement ratios (5 w/%, 10 w/%, 20 w/% and 50 w/% B<sub>4</sub>C) via powder metallurgy and hot pressing to examine their microstructure, hardness and dry-sliding-wear performance. Powder compositions were verified with XRD and the microstructure of the sintered composites was evaluated using SEM (Scanning Electron Microscope) and EDS analyses. Hardness measurements and dry-sliding-wear tests were performed to evaluate the effect of reinforcement addition on the hardness and wear performance of the fabricated composites. Hot pressing of the composite with 50 w/% B<sub>4</sub>C required a significantly higher sintering pressure at the same sintering temperature. Increasing the B<sub>4</sub>C addition resulted in increased hardness values for all the composites, whereas the lowest worn volume and coefficient of friction were obtained with 10 w/% B<sub>4</sub>C.

**Keywords:** metal-matrix composites, particle size, boron carbide, AZ91, material characterization, SEM, hardness, dry sliding wear

Avtorji so izdelali AZ91-B<sub>4</sub>C kompozite z različno vsebnostjo ojačitvene faze (5, 10, 20 in 50) w/% B<sub>4</sub>C s pomočjo postopkov metalurgije prahov in vročega stiskanja. Sledila je preiskava njihove mikrostrukture, določitev trdote in odpornosti proti obrabi zaradi suhega (nemazanega) drsenja. Sestavo prahu so verificirali z rentgensko strukturno analizo (XRD) in ovrednotili mikrostrukturo sintranih kompozitov z vrstičnim elektronskim mikroskopom (SEM) ter energijsko disperzijsko spektroskopijo (EDS). Meritve trdote in preizkuse obrabe s suhim drsenjem so izvedli zato, da bi določili vpliv dodatka ojačitvene faze na izdelane kompozite. Vročje stisnjen kompozit s 50 w/% B<sub>4</sub>C je zahteval znatnovišji tlak stiskanja pri enaki temperaturi sintranja. Povečanje vsebnosti dodatka B<sub>4</sub>C je povišalo trdoto vseh kompozitov, medtem ko je najmanjši volumen delcev obrabe in najmanjši koeficient trenja imel kompozit z 10 w/% B<sub>4</sub>C.

**Ključne besede:** kompoziti s kovinsko osnovo, velikost delcev, borov karbid, AZ91, materialna karakterizacija, SEM, trdota, suha drsna obraba

## 1 INTRODUCTION

Composites are among the most preferred material types as they provide a combination of the desired characteristics of different materials. Metal-matrix composites (MMCs) constitute a major portion in composite materials. They are generally composed of two constituents, namely the metal matrix and the reinforcement.<sup>1</sup> The main reason for the production of MMCs is to improve the strength, elastic modulus and other mechanical properties of the matrix material via combining the characteristics of metals such as toughness and ductility with the high strength and elastic modulus of ceramics through various methods such as powder metallurgy.<sup>2</sup> Powder metallurgy is a cost-efficient and effective way of obtaining composites with particle or whisker reinforcement.<sup>3</sup> Prior to the production of MMCs with various powder-metallurgy techniques, ma-

trix and reinforcement particles are mixed via various methods. A wide variety of materials can be used as the matrix, thus, composite materials with a wide range of elastic moduli, strengths, and thermal expansion coefficients can be produced. Due to their superior properties, such as high hardness, refractoriness and wear resistance, hard particulates such as B<sub>4</sub>C, SiC, Al<sub>2</sub>O<sub>3</sub>, MgO are widely used as reinforcing agents in MMCs.<sup>4</sup>

Various studies have been introduced on the effect of varying the amount of reinforcement material on the microstructure and wear resistance of the metal-matrix composite fabricated. Wang et al., studied the microstructure and properties such as porosity, hardness and wear resistance of magnesium matrix composites reinforced with 2 w/%, 5 w/% and 7.5 w/% fine TiB<sub>2</sub> ( $\approx 7 \mu\text{m}$ ) particulates.<sup>5</sup> They reported an increase in the hardness of the composites with increasing TiB<sub>2</sub> content, although the increase in hardness was significantly lower in the case of 7.5 w/% fine TiB<sub>2</sub> as a result of its relatively higher porosity content. Yavas and Goller investi-

\*Corresponding author e-mail:  
tuba2111@gmail.com

gated the effect of B<sub>4</sub>C addition (0–5 w/%) on the properties of a TZM alloy produced with spark plasma sintering. They also reported a significant increase in the Vickers hardness of TZM (from 1.9 to 7.8 GPa) by the addition of 5 w/% B<sub>4</sub>C to the TZM.<sup>6</sup> Liu et al. studied the effects of B<sub>4</sub>C addition (1, 2, 3, 5, 7 and 9) w/% on the microstructure and properties of porous alumina ceramics produced with direct selective laser sintering. They used boron carbide to improve the sintering behavior of alumina and they reported a maximum compressive strength for the sintered samples in the case of 7 w/% B<sub>4</sub>C addition.<sup>7</sup> In their research on the effect of in-situ reinforcement on the aging and mechanical behavior of an AZ91 metal-matrix composite, Sahoo and Panigrahi studied the age-hardening kinetics of AZ91 and TiC-TiB<sub>2</sub>/AZ91 composites with different characterization tools, and related the enhanced age hardening kinetics to the presence of a high dislocation density that acted as nucleation sites for Mg<sub>17</sub>Al<sub>12</sub> precipitates.<sup>8</sup> The effect of SiC nanoparticles on manufacturing, microstructure and hardness of Mg-SiC nano-composites was studied by Penther et al., who used 1 and 10 φ/% SiC nano-composites. Reportedly, the nanoparticles pin the grain boundaries and trigger dynamic recrystallization of the Mg matrix.<sup>9</sup>

As mentioned above, the related studies on the use of B<sub>4</sub>C as a reinforcing agent, generally involve minor weight fractions of reinforcement material. The present research, on the other hand, aims to examine the addition of a relatively higher weight fraction (50 %) and to provide a further insight into the hot-pressed AZ91-B<sub>4</sub>C combination on which a scarce number of studies have been encountered, despite their wide applicability in fabrication of composites. In this regard, the microstructure, hardness and dry-sliding-wear performance of metal-matrix composites reinforced with varying weight fractions of B<sub>4</sub>C (5 w/%, 10 w/%, 20 w/% and 50 w/%) were investigated. The produced samples were investigated by means of Scanning Electron Microscopy (SEM), Energy-Dispersive X-ray Spectroscopy (EDS), and then they were subjected to dry-sliding-wear tests under a 5-N load at room temperature, to gain an insight into the dry-sliding-wear performance of the composites produced with hot pressing.

## 2 MATERIALS and METHODS

### 2.1. Powder preparation and characterization

AZ91 was granted by the Esan Company in bulk form. AZ91 magnesium alloy ingot (8 kg) with 637 mm × 139 mm × 70 mm dimensions was initially cut into smaller pieces with a band-sawing machine, and the obtained pieces were machined on a numerical control vertical mill to obtain the material in chip form. Following the machining operation, the obtained chips were ground to obtain finer particles.

The particles obtained after fine milling of the AZ91 ingot were sieved with consecutive mesh sizes (150 μm, 200 μm and 250 μm) and those obtained under 150 μm mesh size were subjected to a particle size distribution analysis. Boron carbide was purchased in powder form from the Bor Optik Engineering R&D Company. The chemical analysis results provided by this supplier show that the boron carbide powder includes 77.96 w/% boron, 20.70 w/% carbon, and 0.31 w/% Fe, and 0.22 w/% boron oxide.

The chemical composition of AZ91 and boron carbide were provided from the suppliers. AZ91 alloy's composition is Mg (88–90.50 %), Be (0.0005–0.0015 %), Al (8.50–9.50 %), Cu (Max. 0.025 %), Ca (Max. 0.010 %), Zn (0.45–0.90 %), Mn (0.17–0.40 %), Ni (Max. 0.001 %), Fe (Max. 0.004 %), Si (Max. 0.050), Sn (Max. 0.010 %), Zr (Max. 0.010 %), Pb (Max. 0.010 %), Ti (Max. 0.010 %), P (Max. 0.010 %).<sup>10</sup>

Both powders were subjected to particle size distribution analysis using a Malvern Mastersizer 3000 device. In the particle size distribution analysis, all the particle size measurements were done in wet mode. Deagglomeration and dispersion of the particles was further ensured through ultrasonic treatment (of 120 s) prior to measurement. In the particle size distribution analysis, AZ91 magnesium alloy's refractive index was 0.900 and dispersant refractive index of water was 1.330. The specific surface area was 88.46 m<sup>2</sup>/kg. The uniformity of the concentration was 0.716. The boron carbide refractive index was 1.570 and the dispersant refractive index of water was 1.330. The specific surface area was 2147 m<sup>2</sup>/kg. The uniformity of concentration was 8.126. The compositions of powders were verified using a RIGAKU SmartLab™ X-ray Diffractometer.

### 2.2. Fabrication of composites with hot pressing

In this work, the metal-matrix composites were obtained via hot pressing of AZ91 and boron carbide powders using a MSE Technology-HP-1200 hot-pressing machine. B<sub>4</sub>C + AZ91 composite powders were prepared by mixing 5 % B<sub>4</sub>C, 10 % B<sub>4</sub>C, 20 % B<sub>4</sub>C and 50 % B<sub>4</sub>C via powder metallurgy. Powder mixtures in 6 gr weight were homogeneously mixed and placed in a mold and subjected to a pressure of 10 MPa, 15 MPa and 45 MPa in the hot-pressing machine for a period of 1 h at 515 °C, as given in **Table 1**. The diameter of the fabricated B<sub>4</sub>C+AZ91 composite samples is 15 mm. After cooling down, the sintered samples were cold mounted and ground with 120, 320, 600 and 1000 grit-size SiC papers prior to microhardness measurements and dry-sliding-wear tests.

### 2.3. Sample characterization and wear tests

Hardness data was acquired using a Qness Q10 (Austria) hardness tester. The average of five micro-hardness measurements and the resulting standard deviations were

**Table 1:** The composite materials and their physical properties

No.	Material	M <sub>i</sub> (g)	M <sub>s</sub> (g)	h (mm)	T <sub>s</sub> (°C)	Press (MPa)
1	AZ91+ B <sub>4</sub> C (% 5)	5.7 g + 0.3 g	4.8 g	17.9 mm	515 (°C)	10 MPa
2	AZ91+ B <sub>4</sub> C (% 10)	5.4 g + 0.6 g	4.8 g	17.3 mm	515 (°C)	10 MPa
3	AZ91+ B <sub>4</sub> C (% 20)	4.8 g + 1.2 g	5.5 g	19.7 mm	515 (°C)	15 MPa
4	AZ91+ B <sub>4</sub> C (% 50)	3.0 g + 3.0 g	5.8 g	21.6 mm	515 (°C)	45 MPa

Mi: Initial mass amount; Ms: Final mass amount; h: Height of samples; Ts: Sintering temperature; Press: Applied press on samples

calculated. To avoid a large scattering of the measured values the highest possible indentation load (HV0.5) was used with 15 s dwelling time. Scanning Electron Microscope (SEM) micrographs and EDS results of the sample cross-sections were obtained using a TESCAN MAIA3 XMU scanning electron microscope. EDS spectra were obtained by taking at least three measurements on the SEM micrographs.

Dry-sliding-wear tests were carried out on a reciprocating pin-on-disk tribometer (Turkyus) using a WC abrader ball (6-mm diameter and 1800-HV hardness) in an atmospheric environment at room temperature. The test parameters were 100-m sliding distance, 0.03-m/s sliding speed and 5-N load (Table 2). The oscillation distance on the test rig was 10 mm. Frictional forces in grams were obtained from the load cell that instantaneously transfers the friction data (with 1 second intervals) to the software of the test rig on a computer system. The obtained frictional forces were used to derive the coefficient of friction graphs using the load parameter.

**Table 2:** Wear parameters

	Parameters	Values
1	Load	5 N
2	Sliding speed	0.03 m/s
3	Sliding distance	100 m

The maximum Hertzian contact pressure was calculated as 787.8 MPa using the following Equation (1) and Equation (2):<sup>11</sup>

$$a = \sqrt[3]{\frac{3F \left[ \frac{1-\nu_1^2}{E_1} - \frac{1-\nu_2^2}{E_2} \right]}{4 \left[ \frac{1}{R_1} + \frac{1}{R_2} \right]}} \quad (1)$$

where *a* is the radius of the contact area; *E*<sub>1</sub> and *E*<sub>2</sub> are the moduli of elasticity, *ν*<sub>1</sub> and *ν*<sub>2</sub> are the Poisson’s ratios, and *R*<sub>1</sub> and *R*<sub>2</sub> are the radii of the sphere (tungsten carbide spherical abrader with 6 mm) and the flat surface (AZ91+B<sub>4</sub>C metal matrix composite, *R* is considered ∞), respectively.

$$P_{\max} = \frac{3F}{2\pi a^2} \quad (2)$$

where *P*<sub>max</sub> is the maximum contact pressure at the centre of the circular contact area, *F* is the applied load and *a* is the radius of the contact area from Equation (1).

The wear volume (volume loss) after each test was measured using a 3D optical profilometer (Huvitz-HDS 5800). The area measurements were taken from two different representative cross-sectional planes that were obtained via five different 3D optical profilometer measurements (Figure 1). The average of the resulting ten area measurements (in square millimeters) was multiplied by the 10-mm oscillation distance to evaluate the approximate wear volumes on each sample surface.

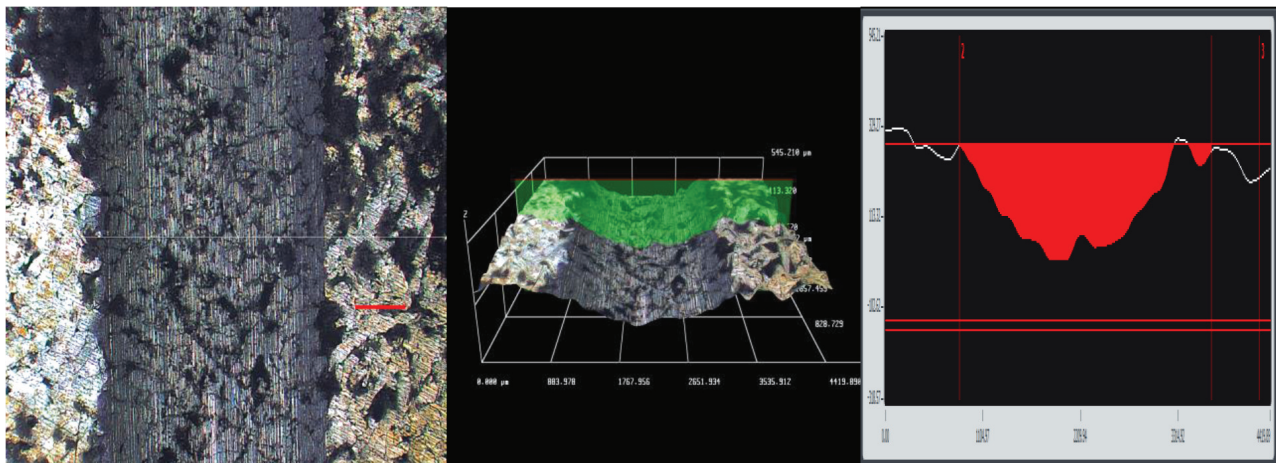


**Figure 1:** 2D and 3D profilometer images of AZ91+ B<sub>4</sub>C (%5)

### 3 RESULTS AND DISCUSSION

#### 3.1. Powder characterization results

The particle size analysis results of boron carbide and AZ91 particles used are given in **Figure 2** and **Figure 3**. The results for B<sub>4</sub>C were obtained as 1.23 μm in D<sub>v</sub> (10), 4.01 μm in D<sub>v</sub> (50) and 127 μm in D<sub>v</sub> (90) as given in **Figure 2**. The results for AZ91 powders were obtained as 40.3 μm in D<sub>v</sub> (10), 126 μm in D<sub>v</sub> (50) and 318 μm in D<sub>v</sub> (90) as given in **Figure 3**.

D<sub>v</sub> (10), D<sub>v</sub> (50) and D<sub>v</sub> (90) correspond to the 10 %, 50 % and 90 % cumulative percentages, which are commonly used in cumulative particle size distribution analysis. D<sub>v</sub> (50) refers to the maximum particle diameter under which 50 % of the sample volume exists, thus it is also referred to as the median particle size. It is possible to observe the significant changes in the main particle size and the extreme points of distribution resulting from the presence of fine or oversized particles/agglomerates by monitoring these three parameters.<sup>12</sup> The uncommon distribution of B<sub>4</sub>C particle size, shown in **Figure 2**, is due to the irregular shapes of B<sub>4</sub>C particles, which is also reported by Liu et al.<sup>7</sup> As seen in **Figure 3**, the AZ91 particles exhibit a relatively more even distribution and this is attributed to the sieving process, which enabled AZ91 particle sizes to be confined within a specific mesh interval.

The XRD analysis results of the boron carbide and AZ91 magnesium alloy powders are shown in **Figure 4**.

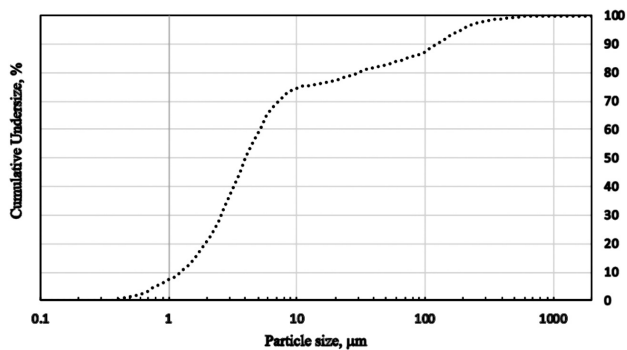


**Figure 2:** Particle size analysis result of boron carbide powder

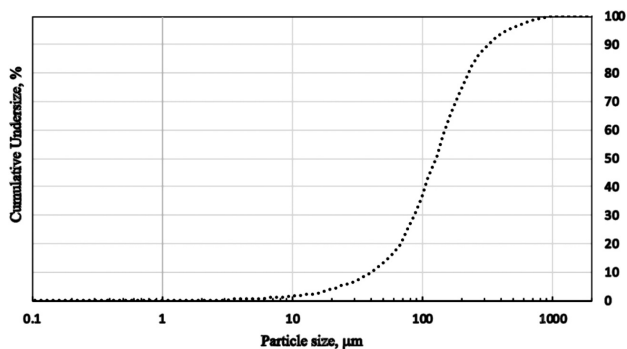


**Figure 3:** Particle size analysis result of AZ91 powder sieved under 150 μm mesh size

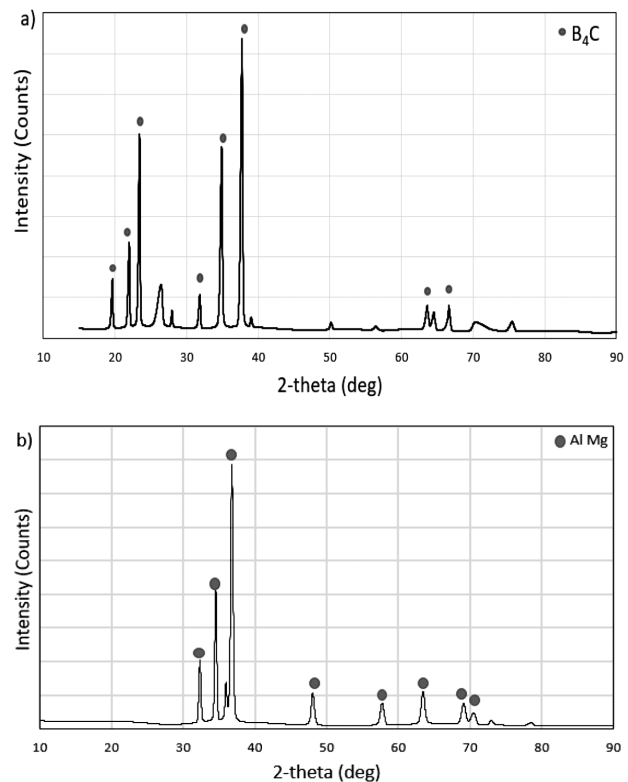


**Figure 4:** Qualitative analysis results by XRD of a) boron carbide and b) aluminum magnesium

The peaks belonging to B<sub>4</sub>C (**Figure 4a**) and aluminium magnesium (**Figure 4b**) verify the compositions of the powders obtained from the suppliers.

#### 3.2. SEM and EDS results

**Figure 5a** to **5d** shows the 500× and 1000× SEM micrographs of AZ91+B<sub>4</sub>C composites with 5 %, 10 %, 20 %, 50 % B<sub>4</sub>C addition, respectively.

In **Figure 5a**, the presence of B<sub>4</sub>C particles is clearly visible in the darker tones. In the figure the particle boundaries of the matrix material are clearly distinguished in the first three samples (**Figures 5a** to **5c**) and they become indistinct in the case of 50 w/% reinforcement ratio (**Figure 5d**). This significant difference in **Figure 5b** is ascribed to the formation and accumulation of dislocations which result in increased grain refinement exerted by the hard B<sub>4</sub>C particulates on the matrix particles as a result of sintering conditions, hence the formation of smaller grains. A similar effect was observed by Singh et al. who synthesized an Al-MWCNT composite to examine the effect of powder milling and reinforcement addition on sintering kinetics and mechanical properties.<sup>13</sup>

During the EDS analysis, spectrum measurements were taken from at least three different points on the specimens and the most representative spectra are shown in **Figure 6**.

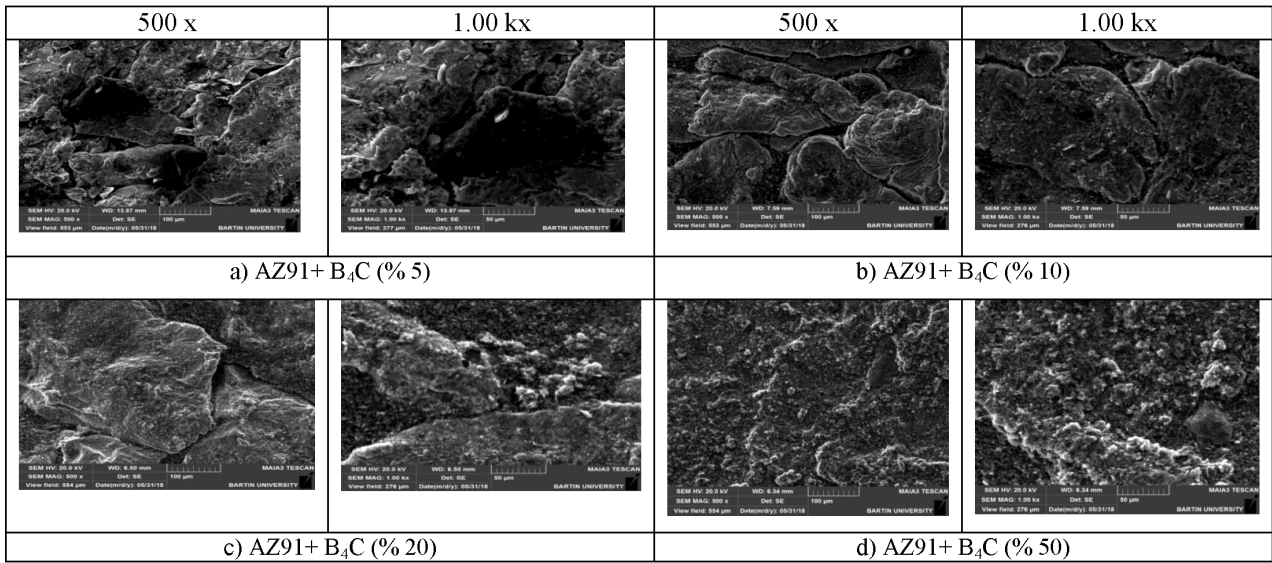


Figure 5: 500× and 1000× SEM micrographs of composites with a) 5 w/%, b) 10 w/%, c) 20 w/%, d) 50 w/% B<sub>4</sub>C addition

The EDS results show that Mg, O, C, B, Al and Zn elements are present in the composition of the alloy. In addition to these elements, remarkable weight fractions of oxygen are observed in all the composite samples. This is attributable to the oxidation of the B<sub>4</sub>C and

Al-Mg composite to a considerable extent on the outer surfaces of composites during the hot sintering process, which took place under atmospheric conditions. As also stated by Çelik and Seçilmiş, particularly Al and its alloys easily react with oxygen to become more stable.<sup>14</sup>

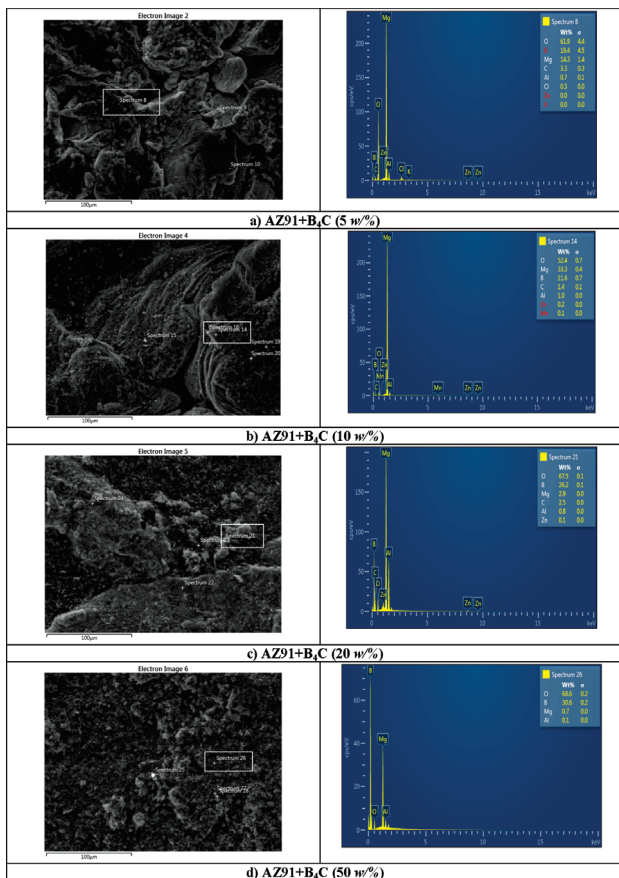


Figure 6: EDS spectra of: a) AZ91 + B<sub>4</sub>C (5 w/%), b) AZ91+B<sub>4</sub>C (10 w/%), c) AZ91+B<sub>4</sub>C (20 w/%), d) AZ91+B<sub>4</sub>C (50 w/%)

### 3.3. Microhardness measurement results

Figure 7 shows the Vickers hardness values of the produced composites. As shown in the figure, the hardness of the produced composites was found as 60.62 HV, 61.38 HV, 65.65 HV and 72.56 HV for 5 w/%, 10 w/%, 20 w/%, and 50 w/% B<sub>4</sub>C addition respectively, which is indicative of increasing hardness by B<sub>4</sub>C addition.

Such contributing effect of hard particulate addition on the hardness of fabricated composites has been repeatedly reported in various studies. Topçu et al. evaluated the effect of B<sub>4</sub>C addition (up to 20 w/%) and sintering temperature on the hardness of the fabricated samples. They attributed the increase in hardness with increasing reinforcement ratio to the dispersion strengthening effect.<sup>15</sup> Likewise, in their research on the effect of particulate reinforcement and heat treatment on the hardness and wear properties of nanocomposites, Sameezadeh et al. reported a considerable increase in the hardness of all composites as compared to the base alloy.

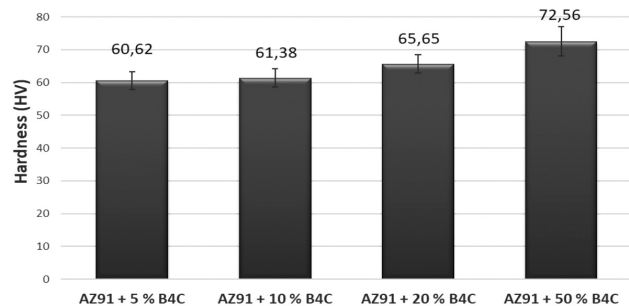


Figure 7: Microhardness measurements of the samples

Reportedly, hard particulates in the composite matrix act as a barrier against dislocation movements within the matrix, thus showing higher resistance against the indenter of the microhardness device.<sup>16</sup>

In the present research the same contributing trend of reinforcement addition on hardness is also encountered, although to an unexpectedly lesser extent. There is a considerable difference between 5 w/% and 50 w/% B<sub>4</sub>C addition, and yet the hardness increased by nearly 19 % (Figure 7). We describe this as follows. Related studies on the utilization of B<sub>4</sub>C and other reinforcing agents generally involve the use of hard particulates at lower ratios (generally under 25 %). The current research, however, involves the use of a significantly higher amount, which is 50 %. Sintering is the consolidation of loose or weakly bonded powders with or without pressure at high temperatures which are close to their melting points.<sup>17</sup> During sintering, hard particulates pin dislocations in the matrix, thus restricting their movement, which improves the hardness of the matrix material through grain refinement. Yin et al. reported such grain refinement and consequent improvement in hardness in which case B<sub>4</sub>C was the matrix material that was reinforced with Ti<sub>3</sub>SiC<sub>2</sub> and Si particles via spark plasma sintering.<sup>18</sup> However, this applies up to a certain weight fraction of the reinforcing agent for the same sintering conditions. In the present case, in which the hard particulates and matrix material have the same weight fraction, a higher sintering pressure was required to achieve the same structural integrity with that of the samples having a lower reinforcement ratio. As also proposed by Xiong et al.<sup>19</sup> densification of B<sub>4</sub>C particulates is a challenging process as a result of its strong covalent bonding and low self-diffusion coefficient. This also arises from the high electron density in inter-atomic regions for B<sub>4</sub>C,<sup>20</sup> hence the reported sintering pressures in Table 1. Although we applied a significantly higher sintering pressure (45 MPa) for the sample with 50 w/% reinforcement, this certainly fell short as we applied the same sintering temperature for all four samples, which in turn resulted in a relatively low difference between the hardness values gained by lowest and highest reinforcement ratios.

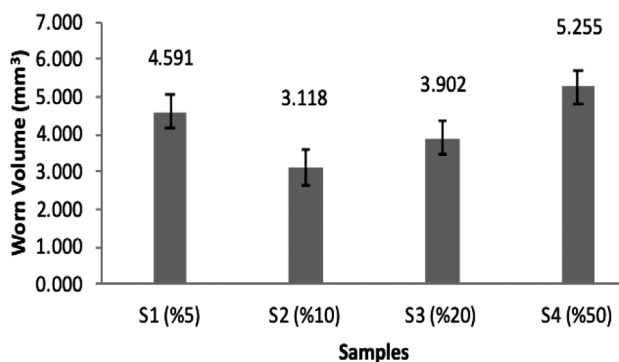


Figure 8: Worn volume graph of samples (S1: 5 w/% B<sub>4</sub>C addition, S2: 10 w/% B<sub>4</sub>C addition, S3: 20 w/% B<sub>4</sub>C, S4: 50 w/% B<sub>4</sub>C addition)

### 3.4. Wear test results

Figure 8 shows the worn volumes of the composites with 5, 10, 20 and 50 w/% B<sub>4</sub>C addition.

As shown in the graph, the worn volumes of the fabricated composites decreased with increasing B<sub>4</sub>C addition for the first two samples and increased with increasing reinforcement ratio after the second sample. The decrease in wear volumes of the first two composites (with 5 w/% and 10 w/% B<sub>4</sub>C) is consistent with Archard's equation, which states that higher hardness results in lower wear rates. Archard, in 1953, formulated this phenomenon with the following equation for wear:

$$W = k \frac{P_n s}{H} \quad (2)$$

As indicated by the equation, the volume of the material removed (W) is directly proportional to the sliding distance (s), normal pressure (p) and the dimensionless wear coefficient (k), and inversely proportional to the hardness of the surface being worn away (H).<sup>21</sup> In addition to Archard's approach, hard reinforcement materials are also reported to affect the contact area between sliding counterparts which leads to reduced wear rates during sliding.<sup>22</sup> Turan et al. likewise evaluated the effect of B<sub>4</sub>C and SiC particle reinforcements on the wear properties of magnesium matrix metal composites.<sup>23</sup> They also reported that, increasing B<sub>4</sub>C addition decreased the specific wear rates under a 5-N load. In another research, Uthayakumar et al. also reported an increase in the wear resistance of Al-SiC-B<sub>4</sub>C hybrid composites with the addition of SiC and B<sub>4</sub>C particles.<sup>24</sup>

The other two samples, however, exhibited increased wear volumes with increasing B<sub>4</sub>C amount and sample 4 with 50 w/% reinforcement ratio displayed the lowest wear resistance. Such a compromise in wear performance despite increasing hardness in the composites with reinforcement addition is also reported by other researchers. Çelik and Seçilmiş proposed that, although increasing reinforcement ratio continuously increases the hardness and other mechanical properties of composites,

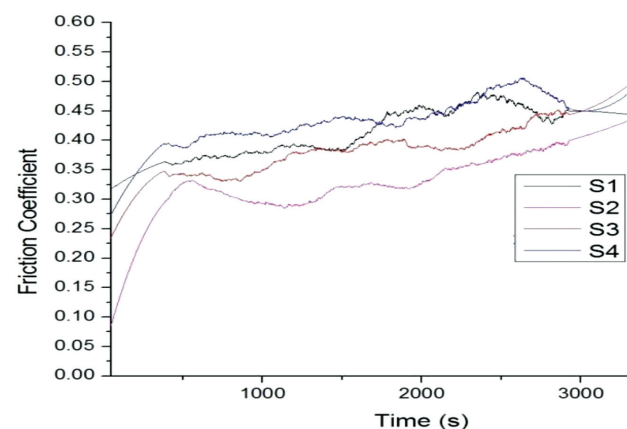


Figure 9: Friction-coefficient graphs of samples (S1: 5 w/% B<sub>4</sub>C addition, S2: 10 w/% B<sub>4</sub>C addition, S3: 20 w/% B<sub>4</sub>C, S4: 50 w/% B<sub>4</sub>C addition)

wear performance is improved only up to a certain volume fraction.<sup>14</sup> Likewise, Baradeswaran and Elaya Perumal reported in their research related to the influence of B<sub>4</sub>C on tribological and mechanical properties of Al7075/B<sub>4</sub>C composites that the best wear performance was obtained by 10 w/% B<sub>4</sub>C addition among (5, 10, 15, and 20) w/% B<sub>4</sub>C addition, which is quite the same case with the current study.<sup>25</sup> We further propose that, such an increase in the worn volume in the samples with 20 and 50 w/% B<sub>4</sub>C addition is attributable to the need for higher sintering conditions (sintering temperature and pressure) to obtain the same structural integrity with the samples having lower B<sub>4</sub>C ratios, as also mentioned in the previous Section 3.3 Microhardness Measurement Results. Despite the significantly higher sintering pressure, the adverse effect of using the same sintering temperature for all samples, on the structural integrity of sample 4 (50 w/% reinforcement), manifested itself to quite a larger extent in the case of wear, as sample 4 exhibited the highest wear volume (**Figure 8**).

**Figure 9** shows the coefficient of friction (COF) values belonging to the composites with 5 w/%, 10 w/%, 20 w/% and 50 w/% B<sub>4</sub>C addition. Friction-coefficient values of all samples were found to vary between 0.075 and 0.5. In the graph, Sample 2 exhibits the lowest COF and Sample 4 exhibits the highest COF, which is indicative of the same trend with wear volumes. In the evaluation of COF values, however, factors other than hot-pressing conditions should be taken into account as COF can be governed by a few other phenomena. During sliding wear, the relative sliding motion of two surfaces that are in contact by the effect of an applied load results in a shear stress, which induces the occurrence of a frictional force. The resulting frictional force depends on various variables including the sliding speed, applied load, the contact area between the surfaces, the temperature rise induced by friction and the various characteristics of mating surfaces.<sup>26</sup> During friction, the exerted normal and shear stresses generate frictional heat which results in the deformation and fracture of asperities, leading to material exchange between the abrader surface and the worn surface, and in turn inducing the formation of a mechanically mixed layer (MML) along with the formation of a boron oxide layer that arises from the oxidation of B<sub>4</sub>C. In their research, Uthayakumar et al. reported the formation of such a tribo-layer that occurred during the wear test of Al–SiC–B<sub>4</sub>C hybrid composites.<sup>24</sup> These together play an important role in the reduction of COF and wear through protecting the material from sub-surface and surface deformation.<sup>24,26</sup> As stated by Singh et al., when this mechanically mixed layer becomes significantly thick, it becomes unstable as the cracks easily form at the subsurface and propagate through the mixed layer, leading to severe wear, which is also referred to as seizure. Reportedly, the formation and thickening of MML happens very fast or does not

happen at all with increased load and sliding-speed conditions.<sup>26</sup>

In the present research, the only variable during the wear tests was the reinforcement ratio and we ascribe the decreasing trend of COF until 10 w/% reinforcement to the maintenance of this layer; and the subsequent increasing trend to the fast-formation or non-formation of this mechanically mixed layer, with increasing B<sub>4</sub>C content. A similar case was encountered by Çelik and Seçilmiş, who investigated the wear behavior of Al matrix composites reinforced with different B<sub>4</sub>C addition.<sup>14</sup> As also elaborated earlier, the sample with 50 w/% lacks structural integrity and ductility as compared to the other samples, thus failing to maintain this lubricating layer due to its relatively more brittle structure.

## 4 CONCLUSIONS

Metal-matrix composites with AZ91 (matrix) and varying B<sub>4</sub>C addition (5 w/%, 10 w/%, 20 w/% and 50 w/%) were fabricated by powder metallurgy and hot pressing and subjected to SEM and EDS analyses and dry-sliding-wear tests to evaluate the effect of B<sub>4</sub>C addition on the microstructure, hardness and wear performance of the sintered composites. As a result, the following conclusions are drawn:

As compared to the other three composites, hot pressing of the composite with 50 w/% B<sub>4</sub>C required a significantly higher sintering pressure (10–15 MPa vs. 45 MPa) at the same sintering temperature (515 °C) than the other composites.

High weight percentages of oxygen were found in the EDS analyses as a result of the high affinity of Al and Mg to oxygen.

Increasing B<sub>4</sub>C addition resulted in increased hardness values for all composites, although the rate of increase in hardness is significantly lower than the increase in reinforcement ratio.

The lowest wear volume and coefficient-of-friction values were obtained with 10 w/% B<sub>4</sub>C, whereas the highest values were obtained with 50 w/% B<sub>4</sub>C.

## Acknowledgment

The authors acknowledge the help of Lecturer Halil EŞGİN in Bartın University Central Research Laboratory Application and Research Center for XRD and SEM analyses. The valuable help of Res. Asst. Fatih AYDIN in Karabuk University-MARGEM is also acknowledged.

Conflicts of Interest: The authors declare no conflict of interest.

## 5 REFERENCES

- 1 T. Ozdemir, The mean grain size determination by ultrasonic velocity technique in basic boron carbide of ceramic metal composites, Afyon Kocatepe University (Master's Thesis), 2006

- <sup>2</sup> M. Kök, Fabrication of 2024 aluminium alloy metal matrix composites reinforced with Al<sub>2</sub>O<sub>3</sub> particles, *Science and Engineering Journal*, 4 (2001) 2, 131–142
- <sup>3</sup> J. M. Torralba, C. E. da Costa, F. Velasco, P/M aluminum matrix composites: an overview, *J. Mater. Process. Technol.*, 133 (2003), 203–206, doi:10.1016/S0924-0136(02)00234-0
- <sup>4</sup> S. M. R. Mousavi, S. M. Abarghouie Seyed Reihani, Investigation of friction and wear behaviors of 2024 Al and 2024 Al/SiCp composite at elevated temperatures, *J. Alloys Compd.* 501 (2010), 326–332, doi:doi.org/10.1016/j.jallcom.2010.04.097
- <sup>5</sup> Y. Wang, H. Y. Wang, K. Xiu, H. Y. Wang, Q. C. Jiang, Fabrication of TiB<sub>2</sub> particulate reinforced magnesium matrix composites by two-step processing method, *Mater. Lett.* 60 (2006) 12, 1533–1537, doi:10.1016/j.matlet.2005.11.065
- <sup>6</sup> B. Yavas, G. Goller, Investigation the effect of B<sub>4</sub>C addition on properties of TZM alloy prepared by spark plasma sintering, *Int. Journal of Refractory Metals and Hard Materials*, 58 (2016), 182–188, doi:10.1016/j.ijrmhm.2016.04.020
- <sup>7</sup> R-Z. Liu, P. Chen, J-M. Wu, S. Chen, A-N. Chen, J-Y. Chen, S-S. Liu, Y-S. Shi, C-H. Li, Effects of B<sub>4</sub>C addition on the microstructure and properties of porous alumina ceramics fabricated by direct selective laser sintering, *Ceramics International*, 44 (2018), 19678–19685, doi:10.1016/j.ceramint.2018.07.220
- <sup>8</sup> B. N. Sahoo, S. K. Panigrahi, Effect of in-situ (TiC-TiB<sub>2</sub>) reinforcement on aging and mechanical behavior of AZ91 magnesium matrix composite, *Materials Characterization*, (2018), doi:10.1016/j.matchar.2018.03.002
- <sup>9</sup> D. Penther, A. Ghasemi, R. Riedel, C. Fleck, S. Kamrani, Effect of SiC nanoparticles on manufacturing process, microstructure and hardness of Mg-SiC nanocomposites produced by mechanical milling and hot extrusion, *Materials Science & Engineering A* 738, (2018), 264–272, doi:10.1016/j.msea.2018.09.106
- <sup>10</sup> <https://www.esanmagnezyum.com/Download/images/AZ91-TDS-EN.pdf>, 19.11.2018
- <sup>11</sup> J. E. Shigley, C. R. Mischke, R. G. Budynas, *Mechanical Engineering Design*, 7<sup>th</sup> ed., McGraw Hill, New York 2004, 161–166
- <sup>12</sup> [https://www.cif.iastate.edu/sites/default/files/uploads/Other\\_Inst/Particle%20Size/Particle%20Characterization%20Guide.pdf](https://www.cif.iastate.edu/sites/default/files/uploads/Other_Inst/Particle%20Size/Particle%20Characterization%20Guide.pdf), 19.11.2018
- <sup>13</sup> L. K. Singh, A. Bhadauria, T. Laha, Al-MWCNT nanocomposite synthesized via spark plasma sintering: effect of powder milling and reinforcement addition on sintering kinetics and mechanical properties, *J Mater Res Technol*, (2018), doi:10.1016/j.jmrt.2018.03.005
- <sup>14</sup> Y. H. Çelik, K. Seçilmiş, Investigation of wear behaviours of Al matrix composites reinforced with different B<sub>4</sub>C rate produced by powder metallurgy method, *Advanced Powder Metallurgy*, 28 (2017) 12, 2218–2224, doi:10.1016/j.apm.2017.06.002
- <sup>15</sup> I. Topcu, H. O. Gulsoy, N. Kadioglu, A. N. Gulluoglu, Processing and mechanical properties of B<sub>4</sub>C reinforced Al matrix composites, *J. Alloy Compd.*, 482 (2009), 516–521, doi:10.1016/j.jallcom.2009.04.065
- <sup>16</sup> M. Sameezadeh, M. Emamy, H. Farhangi, Effects of particulate reinforcement and heat treatment on the hardness and wear properties of AA 2024-MoSi<sub>2</sub> nanocomposites, *Materials and Design*, 32 (2011), 2157–2164, doi:10.1016/j.matdes.2010.11.037
- <sup>17</sup> J. Rojek, S. Nosewicz, M. Mazdziarz, P. Kowalczyk, K. Wawrzyk, D. Lumelskyj, Modeling of a sintering process at various scales, *Procedia Engineering*, 177 (2017), 263–270, doi:10.1016/j.proeng.2017.02.210
- <sup>18</sup> S.-P. Yin, Z.-H. Zhang, X.-W. Cheng, T.-J. Su, Z.-Y. Hu, Q. Song, H. Wang, Spark plasma sintering of B<sub>4</sub>C-TiB<sub>2</sub>-SiC composite ceramics using B<sub>4</sub>C, Ti<sub>3</sub>SiC<sub>2</sub> and Si as starting materials, *Ceramics International*, 44 (2018), 21626–21632, doi:10.1016/j.ceramint.2018.08.245
- <sup>19</sup> Y. Xiong, X. Du, M. Xiang, H. Wang, W. Wang, Z. Fu, Densification mechanism during reactive hot pressing of B<sub>4</sub>C-ZrO<sub>2</sub> mixtures, *Journal of the European Ceramic Society*, (2018), doi:10.1016/j.jeurceramsoc.2018.05.016
- <sup>20</sup> V. Domnich, S. Reynaud, R. Haber, A. M. Chhowalla, Boron carbide: structure, properties, and stability under stress, *J. Am. Ceram. Soc.*, 94 (2011) 11, 3605–3628, doi:10.1111/j.1551-2916.2011.04865.x
- <sup>21</sup> A. Zmitrowicz, Wear patterns and laws of wear – A review, *J. Theo. App. Mech.*, 44 (2006) 2, 219–253
- <sup>22</sup> X. Jiang, N. Wang, D. Zhu, Friction and wear properties of in-situ synthesized Al<sub>2</sub>O<sub>3</sub> reinforced aluminum composites, *Trans. Non-ferrous Met. Soc. China*, 24 (2014), 2352–2358, doi:10.1016/S1003-6326(14)63356-2
- <sup>23</sup> M. E. Turan, H. Zengin, E. Cevik, Y. Sun, Y. Turan, H. Ahlatci, Wear behaviors of B<sub>4</sub>C and SiC particle reinforced AZ91 magnesium matrix metal composites, *World Academy of Science Engineering and Technology International Journals of Materials and Metallurgical Engineering* 10 (2016) 9, 1224–1227
- <sup>24</sup> M. Uthayakumar, S. Aravindan, K. Rajkumar, Wear performance of Al-SiC-B<sub>4</sub>C hybrid composites under dry sliding conditions, *Mater. Des.*, 47 (2013) 456–464, doi:10.1016/j.matdes.2012.11.059
- <sup>25</sup> A. Baradeswaran, A. Elaya Perumal, Influence of B<sub>4</sub>C on the tribological and mechanical properties of Al 7075-B<sub>4</sub>C composites, *Composites Part B: Engineering*, 54 (2013), 146–152, doi:10.1016/j.compositesb.2013.05.012
- <sup>26</sup> M. Singh, B. K. Prasad, D. P. Mondal, A. K. Jha, Dry sliding wear behaviour of an aluminium alloy-granite particle composite, *Tribology International*, 34 (2001), 557–567